XPS study of InP/InGaAs/InGaAsP microstructures irradiated with ArF laser in air and deionized water

Neng Liu[1], Khalid Moumanis[1], Sonia Blais[2], Jan J. Dubowski[1]*

[1]Laboratory for Quantum Semiconductors and Photon-based BioNanotechnology, Department of Electrical and Computer Engineering, Université de Sherbrooke, Québec, Canada J1K 2R1
[2]Centre de caractérisation des matériaux, Université de Sherbrooke, Québec, Canada J1K 2R1

*URL: http://www.dubowski.ca

ABSTRACT

Excimer lasers, due to their compatibility with a large-scale industrial production, are attractive tools for precise processing of photonic and microelectronic materials. In this article, we discuss the effect of ArF excimer laser defect formation on the surface of InP/InGaAs/InGaAsP quantum well (QW) microstructures irradiated in air and deionized (DI) water environments. Structural defects on surfaces of such QW materials have been known to induce vacancy diffusion towards the QW region and lead to the so called quantum well intermixing (QWI) effect during the rapid thermal annealing step. Excimer lasers have been used to create surface defects on InP/InGaAs/InGaAsP microstructure and induce QWI during high temperature annealing. Chemical composition of the QW microstructures irradiated with ArF laser in air and DI water is studied with X-ray photoelectron spectroscopy to investigate both the formation and role of the surface defects in the laser-induced QWI process.

Keywords: InP/InGaAs/InGaAsP quantum well microstructures, ArF excimer laser radiation, quantum well intermixing, X-ray photoelectron spectroscopy

1. INTRODUCTION

InP based quantum well (QW) microstructures, such as InP/InGaAs/InGaAsP, are important materials for photonic devices operating in the near-infrared region of an electromagnetic spectrum. A semiconductor wafer with as-grown QW microstructure, typically, represents same-bandgap material. Functioning of active photonic devices, such as arrays of multi-color lasers and modulators, however, requires different bandgap materials. The most frequently used approach allowing fabrication of multi-bandgap wafers is based on an epitaxial growth/re-growth technique, although the fabrication of such wafers at an attractive cost has remained a challenging task. Post-growth processing that employs so-called quantum well intermixing (QWI) has been investigated to address this issue.[1, 2] Defect-driven QWI has remained a challenging task, mainly due to the difficulties in controlling the nature, concentration and location of defects induced by ion implantation[3], impurity doping[4] or dielectric layer (SiO_2/Si_3N_4) coating.[5] The application of excimers for that purpose brings advantages related to the strong optical absorption of these lasers, e.g., ArF at 193 nm, KrF at 248 nm and XeCl at 308 nm, in InP and GaAs – materials that have been employed for capping most of the III-V QW microstructures. For instance, the strong absorption of InP, reaching about 10^6 cm^{-1} the UV spectral region[6], allows creating defects confined to the near surface, typically less than 10 nm deep. Excimer lasers have already been applied in manufacturing processes of semiconductor devices[7], thus they are suitable for a relatively large-scale production. An early study of excimer lasers used for selected area defect formation have revealed feasibility of this approach for QWI and selected-area bandgap engineering.[8, 9,10] The full quantitative description of the process, however, has been missing. The progress in that context is important as the properties of future photonic devices, made from the laser processed material, are expected to depend on the nature of laser-induced defects and microstructural properties of laser modified surface, similarly, e.g., to the dependence of the performance of metal-semiconductor contacts on the properties of semiconductor surfaces.[11] Irradiation of InP surface with an ArF laser (λ=193 nm) in an air environment leads to the increase, in proportion to the number of laser pulses, of both the indium (In)/phosphorus (P) atomic ratio and thickness of the laser induced oxide layer.[9] This results in an increased concentration of P vacancies and In interstitials that will diffuse towards the QW

Synthesis and Photonics of Nanoscale Materials IX, edited by Frank Träger, Jan J. Dubowski, David B. Geohegan,
Proc. of SPIE Vol. 8245, 82450E · © 2012 SPIE · CCC code: 0277-786X/12/$18 · doi: 10.1117/12.913082

region during a rapid thermal annealing (RTA) step and, consequently, enhance intermixing between the QW and barrier materials.[8,12] The surface chemical composition of laser irradiated material is expected to be affected by the irradiation environment. For instance, X-ray photoelectron spectroscopy (XPS) data showed that irradiation of InP with a KrF laser in an NH_3 environment leads to the formation of InN_x and PN_x compounds on the surface of this material.[11]

We have recently reported that surface morphology of the excimer laser irradiated InP material remains relatively unaffected if processed with laser fluence and pulse number not exceeding 95 mJ/cm^2 and 100, respectively.[13] In this work, we investigate chemical composition of InP cap material grown epitaxially on InGaAs/InGaAs/InP QW microstructures and irradiated with an ArF excimer laser in air and deionized (DI) water environments. Our primary interest is focused on finding the correlation between chemical state of the sample surface and observed amplitude of the QWI effect.

2. EXPERIMENT

The investigated InP/InGaAs/InGaAsP microstructure was grown on n-doped InP (001) substrate and it was designed to emit at 1.540 μm at room temperature. The microstructure comprises of five (5) 6-nm-thick $In_{0.47}Ga_{0.53}As$ QWs separated by four (4) 10-nm-thick $In_{0.74}Ga_{0.26}As_{0.57}P_{0.43}$ barriers. The optical confinement is provided by 110 and 20 nm thick InGaAsP graded bandgap materials interfacing the substrate and surface side of the QW stack. The whole microstructure was capped with a 30-nm thick InP layer. A cross-section with details of the investigated microstructure is shown in Figure 1. Samples, typically 5 mm*5 mm, were cleaved from a wafer and cleaned with standard solvents. The samples were installed in a 0.74-mm-tall chamber equipped with a fused silica window that transmitted at least 90% of radiation in the UV region. The irradiation of samples was carried out either in air or DI water environments.

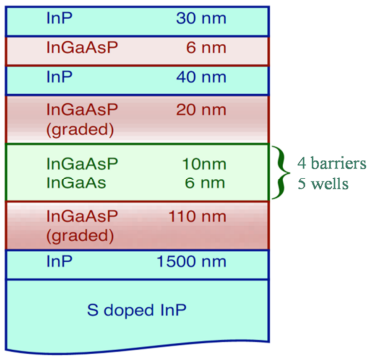

Figure 1. Schematic cross-section of the investigated InP/InGaAs/InGaAsP microstructure.

Irradiation was carried out with an ArF (193 nm) laser (Lumonics, Pulse Master 800) equipped with a beam delivery system for mask projection with a 2.6 demagnification ratio. A double micro-lens fly-eye-array homogenizer was used to shape the laser beam used to project a circular mask on the sample surface. With a computer controlled X-Y-Z-Theta positioning of the sample, the setup allowed for the processing of the same sample at numerous sites. Following the UV laser irradiation, samples were installed in a sealed nitrogen container to limit their exposure to an atmospheric environment, and transported for further processing.

After laser irradiation, the samples were annealed for 2 min at 700°C in a rapid thermal annealing (RTA) furnace (JIPELEC, Jetfirst) in an atmosphere of mixed hydrogen and nitrogen forming gas (N_2:H_2=1:9).

The XPS measurements were performed by using spectrometer (Kratos Analytical, AXIS Ultra DLD) with Al Kα as a source operating at 150W, with a base pressure of $1x10^{-9}$ Torr. The surface survey scan and high resolution scans were observed in constant energy modes at 50 eV and 20 eV pass energy, respectively. The size of an analyzed area on the investigated samples was set at 220 μm*220 μm. The XPS spectra were processed using Casa XPS 2.3.15 software. To compensate the surface charging effect, all XPS data binding energies were referenced to the adventitious C 1s peak at

the binding energy (BE) of 285.0 eV.[14] For spectral fitting, Gaussian-type and asymmetric peaks with constant full width at half-maximum (FWHM) were used for all components at a particular peak envelope.[15] Quantification of XPS data was obtained by determining the area under each component peak that was corrected using manufacturer's relative sensitivity factors (RSF). The RSF used for In 3d, P 2p and O 1s were 13.3, 1.19 and 2.93, respectively. XPS analysis of the cap InP surface of InP/InGaAs/InGaAsP microstructure was carried out for both laser irradiated and RTA samples.

Room temperature photoluminescence (PL) measurements of investigated samples were carried out with a commercial mapper (Philips, PLM-150) that employs a Nd:YAG laser to excite the samples. The PL signal was dispersed by a monochromator and detected by an InGaAs photodiode array. The PL maps were obtained based on the QW electron-hole recombination peak, which for the as-grown material was located at 1540 nm. The PL maps were collected with a spatial resolution set at 30 μm.

3. RESULTS AND DISCUSSIONS

3.1 XPS analysis of sample irradiated by ArF laser in air and DI water

Figure 2 shows the In 3d 5/2 (a), P 2p (b), C1s (c), O 1s (d) and expanded O 1s (e) XPS spectra of an InP cap of as-grown the InGaAs/InGaAsP/InP microstructure. The results indicate the surface presents different oxides as the In 3d 5/2 spectrum can be fitted with seven peaks assigned to In-In-C (BE=442.7±0.2eV, FWHM=0.67eV), elemental indium, In-In (BE=443.5±0.2eV, FWHM=0.67eV), InP (BE=444.4±0.1eV, FWHM=0.67eV), indium oxide, InO_x (BE=445.2±0.2eV, FWHM=0.67eV), $In_x(PO_4)$ (BE=445.5±0.1eV, FWHM=0.67eV), $In(PO_3)_y$ (BE=446.0±0.2eV, FWHM=0.67eV) and $In(PO_3)_3$ (BE=446.4±0.2eV, FWHM=0.67eV).[15,16] All the peaks are fitted with Gaussian functions, except for the elemental In, where an asymmetric function was used.[17]

The In-In-C peak is clearly observed in the C 1s spectrum in Figure 2 (c). This peak, located at 282.7eV±0.2eV, is assigned to the formation of metal carbide.[18] However, as the electron negativity of C (2.5) is higher than P (2.1), In-In-C binding energy should be higher than that of InP. However, as the peak at lower binding energy (442.7±0.2eV) in In 3d 5/2 appears accompany with appearance of the carbide peak in C 1s spectrum, we ascribed these peaks as indium carbide, In-In-C.[19,20] The presence of InO_x, $In_x(PO_4)$, $In(PO_3)_y$ and $In(PO_3)_3$ has been identified at higher binding energies[18,21,22], as shown in Figure 2. The P 2p spectrum shows 2p 3/2 and 2p 1/2 doublets for each element or chemical compound (indicated in Figure 2 (b) for InP only). The doublet separation and branch ratio of P 2p 3/2 to P 2p 1/2 were fixed at 0.85 and 2.0, respectively.[23] The peaks at BE=128.6±0.2eV (FWHM=0.56±0.1 eV) and at BE=129.2±0.1eV (FWHM=0.56±0.1eV) were assigned to phosphorus in InP.[24]

The oxides at the higher binding energy can be ascribed to $In_x(PO_4)$ (BE=133.1±0.2eV, FWHM=1.1±0.1eV), $In(PO_3)_y$ (BE=133.8±0.2eV, FWHM=1.1±0.1eV) and $In(PO_3)_3$ (BE=134.4±0.2eV, FWHM=1.1±0.1eV) which are consistent with those in the In 3d 5/2 spectra.[22,21,25] There are two small peaks at lower binding energy (132.2±0.2eV) ascribed to Na_3PO_4, which is possible from contamination during experiment and handling.[26] In C 1s XPS spectrum in Figure 2 (c), the C (adv) was set to 285.0eV which was used for the calibration of charging effect. Besides In-In-C peak, C spectrum also showed the presence of three additional C absorbates species, alcohol –COH (286.5±0.2eV), carbonyl –CO (287.9±0.1eV) and ester –COO- (288.8±0.1eV).[27] Four small peaks corresponding to these O-containing C absorbates were shown in O 1s spectrum in Figure 2 (d). The intensities of these peaks were related to the corresponding species in C 1s spectrum in Figure 2 (c). Identification of these C absorbates species in the O 1s peak is important to analyze the quantities of indium oxides and InP oxides (InP_xO_y, including $In_x(PO_4)$, $In(PO_3)_y$ and $In(PO_3)_3$, whose O 1s peaks binding energy is close). The expanded O 1s peak at higher binding energy was shown in Figure 2 (e). The four small C absorbates species –COH (532.9±0.2eV), -CO (532.3±0.1eV), and –COO- (532.3±0.3eV, 533.6±0.2eV) peaks were shown in dash line. Besides these peaks, one peak (531.9±0.2eV) was ascribed to absorbed oxygen species and the other peak (533.7±0.2eV) was ascribed to bridging oxygen atoms in $In(PO_3)_y$ and $In(PO_3)_3$.[22,28]

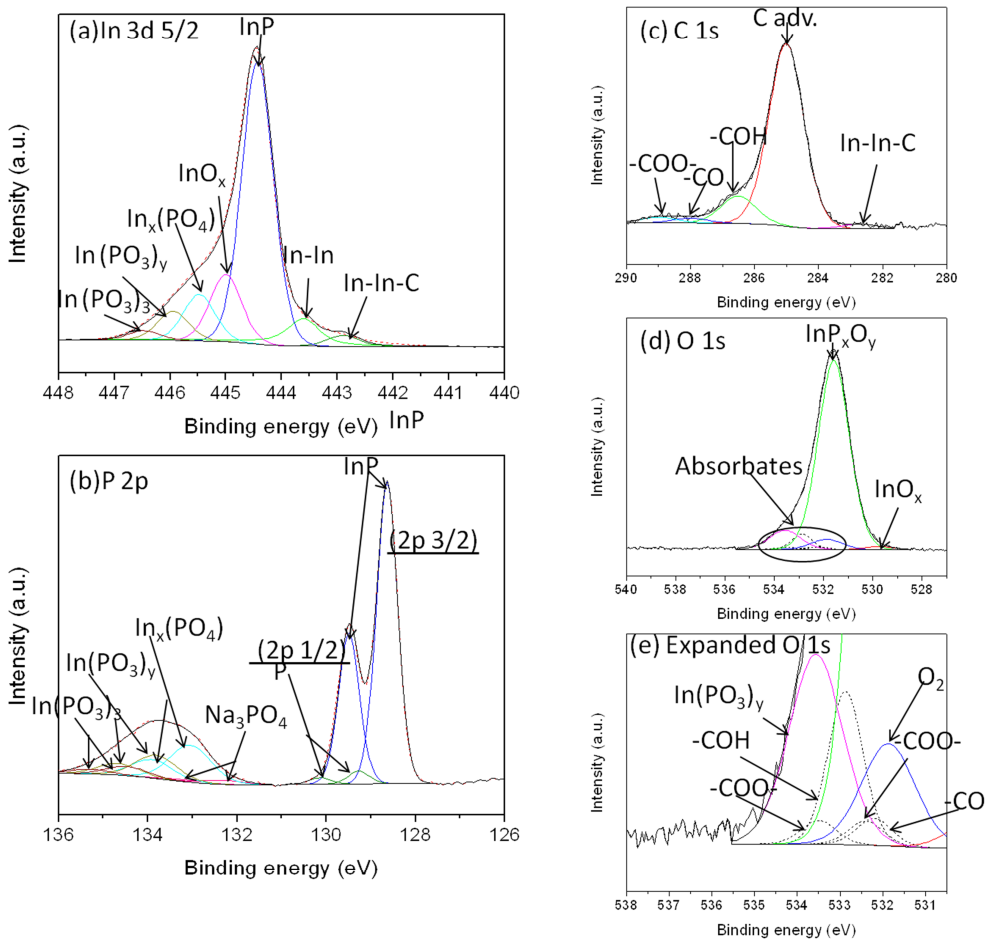

Figure 2. (a) In 3d 5/2, (b) P 2p, (c) C1s and (d) O 1s XPS spectra of as grown InP surface of InP/InGaAs/InGaAsP microstructure before laser irradiation. The expanded view of O 1s was shown in (c).

Figure 3 shows the In 3d 5/2 and P 2p XPS spectra of InP/InGaAs/InGaAsP microstructure irradiated by ArF laser in DI water (a-b) and in air (c-d) with 20 pulses at 82 mJ/cm^2. Both irradiated sites show InP, InO_x and InP_xO_y (including $In_x(PO_4)$, $In(PO_3)_y$). But the $In(PO_3)_3$ peak can only be identified on the site irradiated in air. However, in contrast to the as-grown material, the site irradiated in DI water shows no peaks at BE=446.4±0.2eV in In 3d 5/2 spectrum and at BE=134.4±0.2eV in the P 2p spectrum indicating a significantly disappearance of $In(PO_3)_3$. The likely reason for the reduced concentration of InP_xO_y is a relatively large solubility of phosphorous oxides in DI water[29]. In-In-C peak at lower binding energy in In 3d 5/2 spectrum has also disappeared obviously on site irradiated in DI water. However, a significantly increased intensity of XPS signals related to In-In-C as well as InP oxides has been observed on the site irradiated by ArF laser in air (Figure 3 (c)).

Using a model reported in the literature[30], our COMSOL calculations indicate that the peak temperature of InP irradiated with ArF laser at 82mJ/cm^2 in air is about 500 K. This condition leads to the formation of indium oxides and InP oxides by adsorption of oxygen that enters the In-In and In-P bonds.[31] It has been suggested that InP oxides are formed by the P atom outdiffusion from bulk material through the oxide layer and reaction with oxygen, leaving group V vacancies in the InP based heterostructure.[32] The presence of such vacancies will promote atomic interdiffusion at sufficiently high

temperatures induced in the RTA step. In contrast, the irradiation in DI water using same laser fluence and pulse number induces a peak temperature of about 360 K. At this temperature, no significant decomposition of InP is expected while the DI water environment will enhance desorption of phosphorous oxides by the dissolution process. This should result in a reduced concentration of group V vacancies and possibly a weaker atomic interdiffusion at the RTA step. Indeed, as discussed later in this report, we have observed systematically reduced amplitudes of the QWI effect in samples irradiated in DI water in comparison to those irradiated in air.

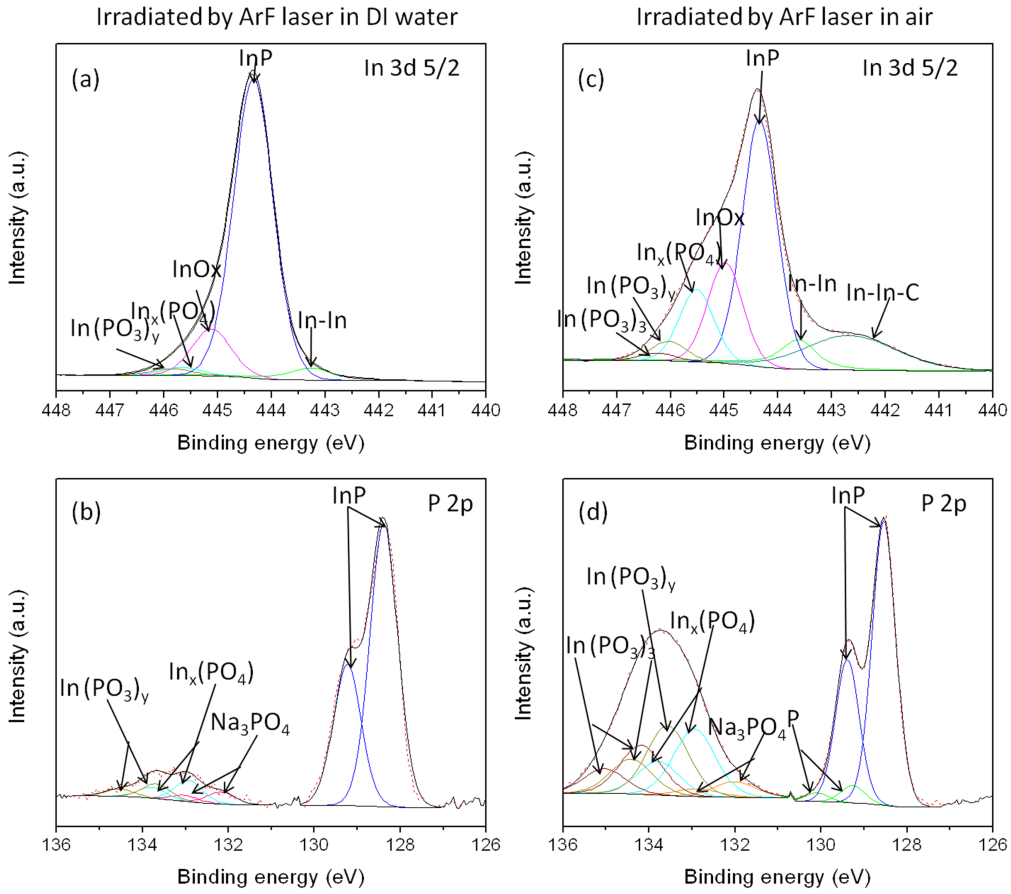

Figure 3. In 3d 5/2 and P 2p XPS spectra of sample irradiated by ArF laser in DI water (a), (c) and in air (b), (d) with 20 pulses at 82mJ/cm^2.

Figure 4 shows the C 1s (a), O 1s (b), O 1s expanded (c) XPS spectra of a sample irradiated in DI water and in air. It can be seen that intensity of InP_xO_y peak and that of the InO_x peak has increased compared with O 1s spectrum of non-irradiated sites (see Figure 2d). There are same C absorbates, including -COH, -CO and –COO- on both two irradiated sites. The higher intensity of In-In-C carbide in the C 1s spectrum is consistent with the increase of In-In-C in In 3d 5/2 XPS spectrum of sample irradiated in air, see Figure 3 (c). However, the carbide peak disappeared in the sample irradiated in DI water. The expanded view of the O1s spectrum (Figure 4c) of the sample irradiated in DI water shows the presence of the H_2O peak at BE=536.0±0.2 eV that was reported, e.g., for a rhenium sample irradiated in DI water.[33]

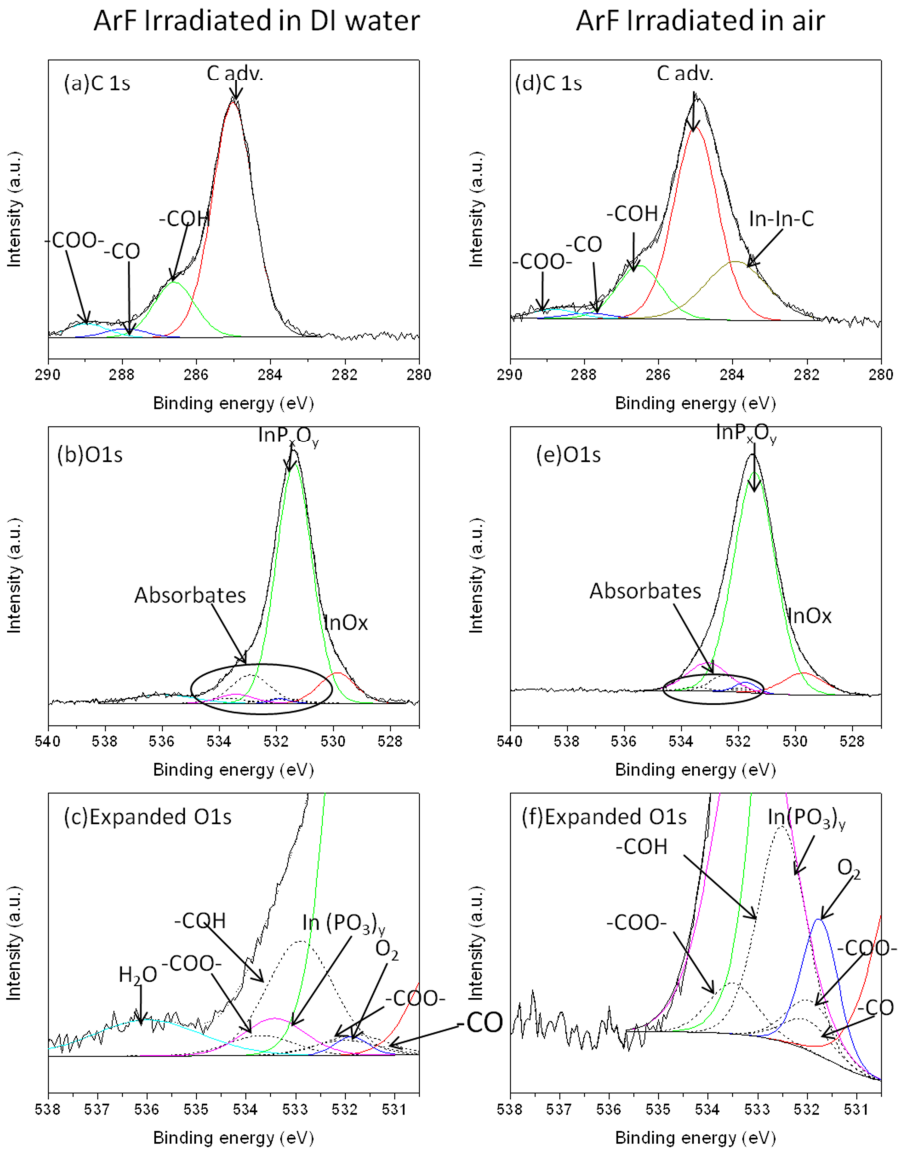

Figure 4. C 1s and O 1s XPS spectra of samples irradiated by ArF laser in DI water (a), (b) and in air (d), (e). The expanded views of O 1s are shown in (c) and (f).

Figure 5 shows In 3d 5/2 and P 2p XPS spectra of sites after ArF laser irradiation in DI water (a), (b) and in air (c), (d) and RTA. We find that in both cases the RTA step leads to a decreased amount of surface oxides (compared with Figure 3). The reduction of oxides after RTA is expected due to the decomposition process. For instance, P evaporates at 650°C[34], and chemical reaction of oxides with H_2 is also expected to reduce their presence on the InP surface.[35] In the In 3d 5/2 spectrum (Figure 5c), we find that the site irradiated in air shows the peak associated with In-In-C decreased significantly and shifted by 0.5 eV when compared to the In-In-C peak observed before RTA (see Fig. 4d). This behavior may be related to formation of a new-phase material as carbides are known to reconstruct when exposed to H_2 annealing at temperatures exceeding 650°C.[36] Compared with the defects diffusion rate ($2.3*10^{-15}$ $cm^{-2}s^{-1}$) on similar InGaAs QW structure during pulsed Nd:YAG laser QWI [37], the diffusion coefficient of C in GaAs is relatively low (< 10^{-16} cm^2s^{-1}).[38]

Thus, we disregard diffusion of this element towards the QW region as a plausible mechanism contributing to the QWI effect.

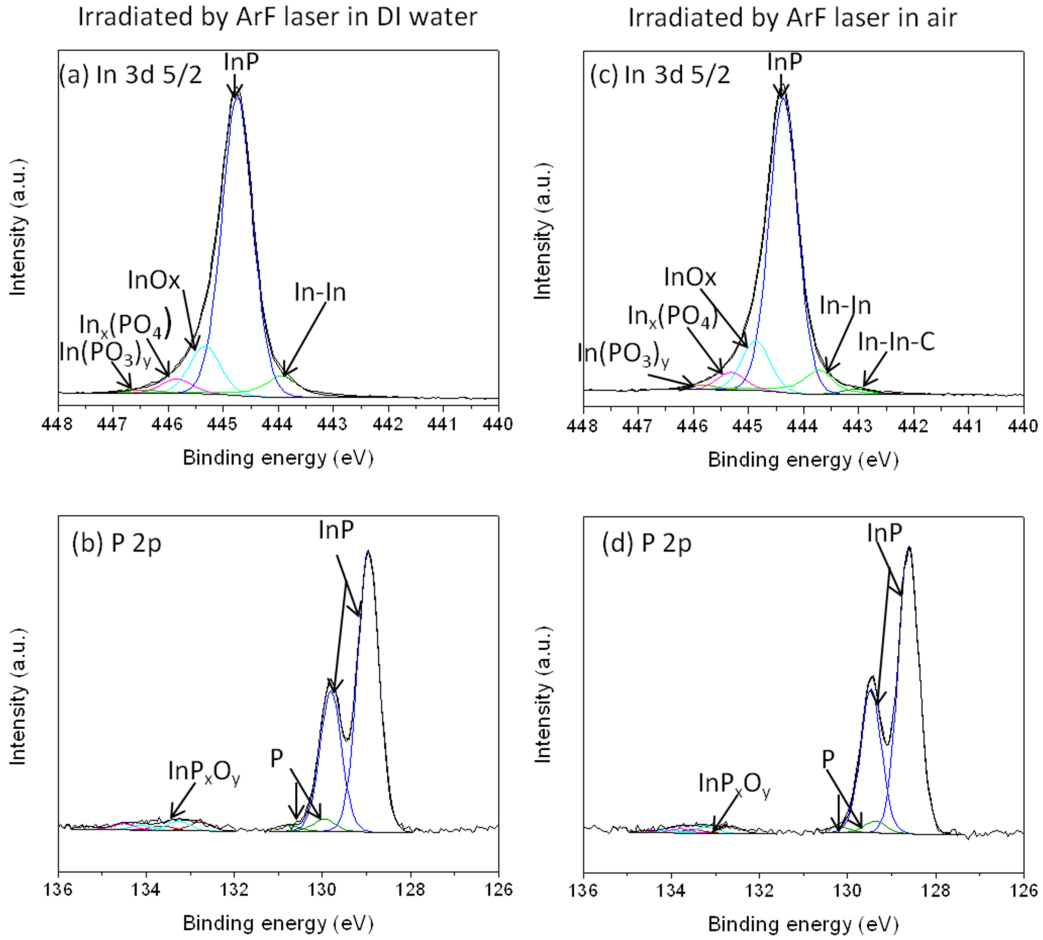

Figure 5. In 3d 5/2 and P 2p XPS spectra of ArF laser irradiated sites in DI water (a), (b) and in air (c), (d) and RTA at 700°C for 2 minutes.

Figure 6 shows the C 1s and O 1s XPS spectra of sites ArF laser-irradiated in DI water (a, b) and in air (c, d) following RTA at 700°C for 2 minutes. It can be seen that the H_2O related features observed in Figure 4, have disappeared as a result of the annealing. Also, as a result of this processing step, the InP_xO_y peak intensity has decreased significantly, and the In-In-C feature in the C 1s peak irradiated in air is practically invisible.

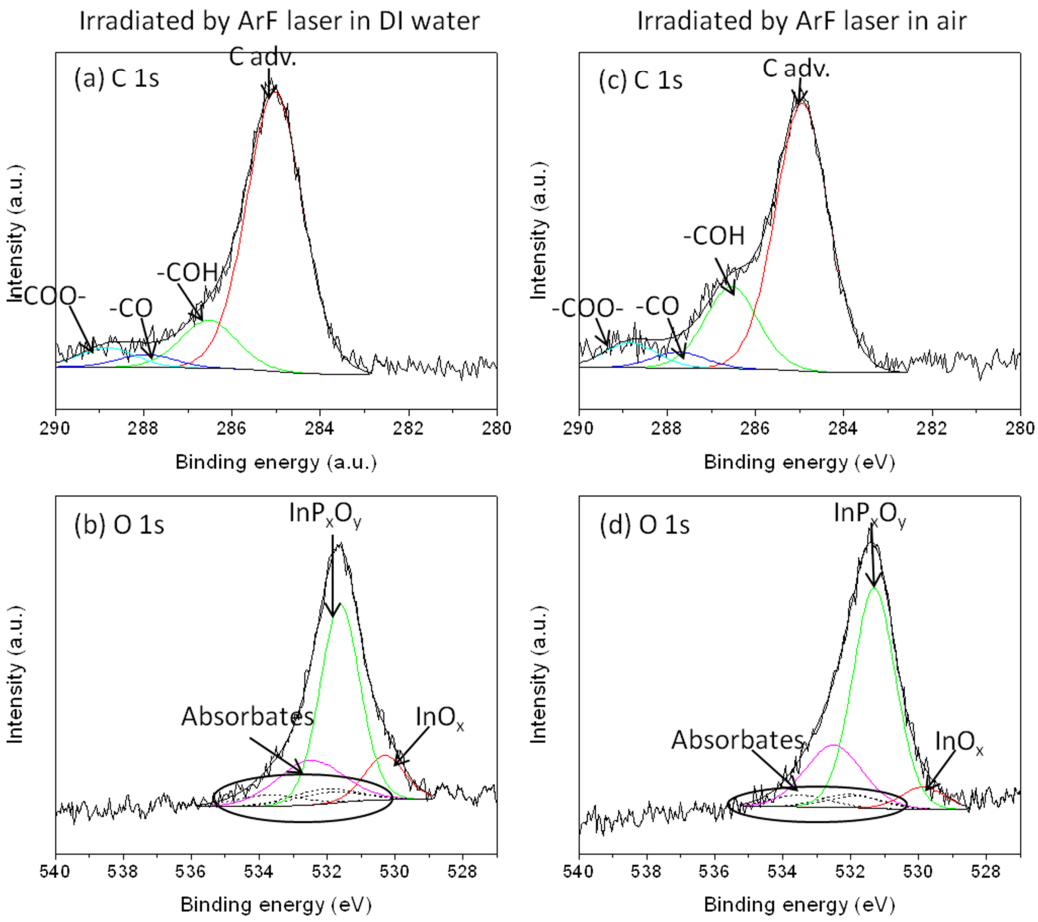

Figure 6. C 1s and O 1s XPS spectra of sites irradiated with ArF laser in DI water (a), (b) and in air (c), (d) and RTA at 700°C for 2 minutes.

Figure 7 shows a laser pulse number dependence of the chemical composition of InP cap in the InP/InGaAs/InGaAsP QW microstructure for the ArF irradiation at 82 mJ/cm^2 in DI water (a) and air (b). It can be seen that concentration of C adsorbates decreases slightly with the pulse number, which demonstrates the laser cleaning effect. Also, the irradiation in air seems to produce samples with relatively lower concentration of C absorbates on their surface. More importantly, the results demonstrate that the irradiation in air produces samples with higher concentration of InP_xO_y, more than 2 times greater than that observed in samples irradiated in DI water. As the X-ray probing depth is around 10 nm, the increasing concentration of InP_xO_y explains a decay of the InP XPS signal clearly observed especially for the samples irradiated in air. The process of an excimer laser-induced oxide formation on InP in an oxygen (air) atmosphere is similar to that of an excimer laser-induced nitridation on InP in an ammonia atmosphere.[39]

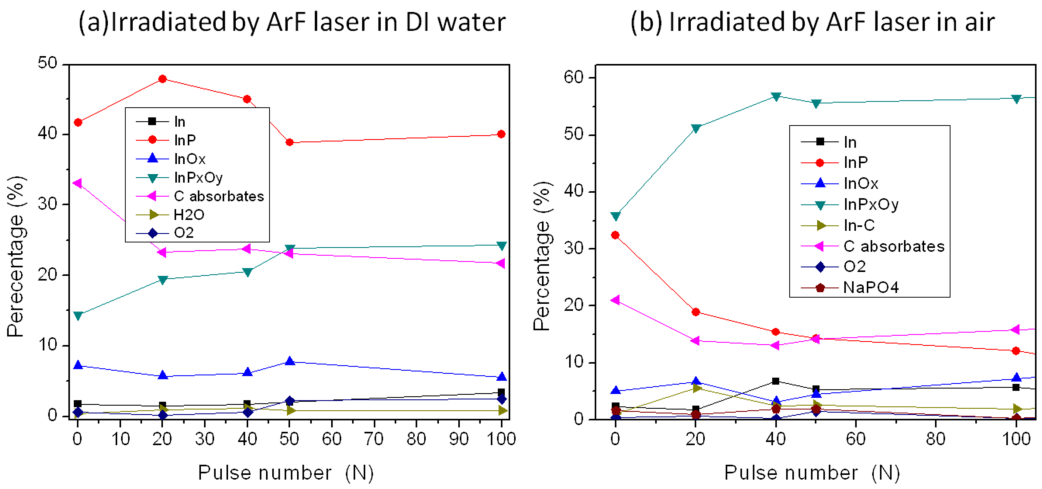

Figure 7. Chemical composition of InP cap in the InP/InGaAs/InGaAsP QW microstructure as a function of the ArF pulse number for the irradiation in DI (a) water and air (b).

Figure 8 illustrates a laser pulse number dependence of the chemical composition of the InP cap in the InP/InGaAs/InGaAsP QW microstructure that was irradiated ArF laser at 82 mJ/cm^2 in DI (a) and air (b) and RTA at 700°C for 2 minutes. It can be seen that the annealing step has restored chemical composition of the laser-irradiated material (N = 100 pulses), regardless of the irradiation environment, to that observed for the initial surface (N = 0). The results indicate that the ArF laser irradiation at 82 mJ/cm^2, and at least up to 100 pulses, does not cause significant degradation of the InP material.

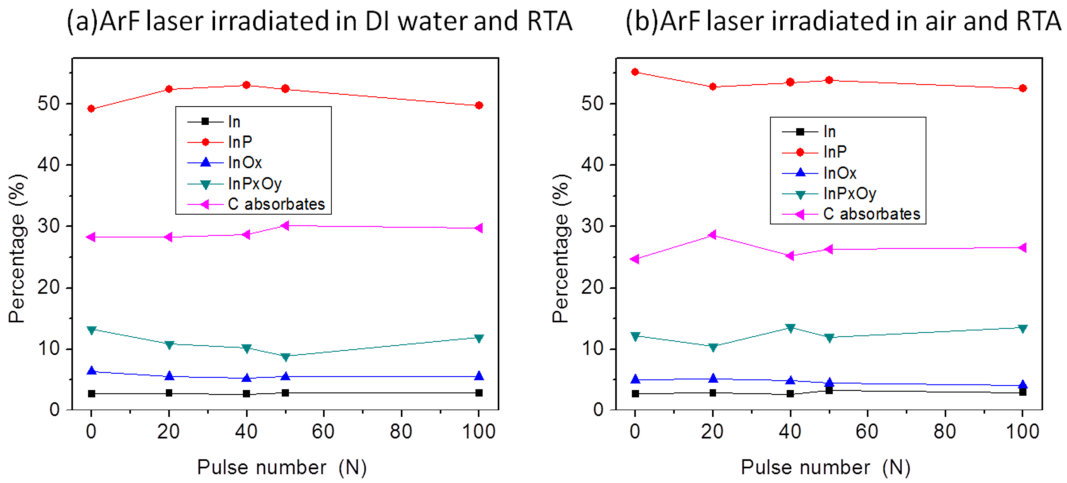

Figure 8. Chemical composition of InP cap in the InP/InGaAs/InGaAsP QW microstructure as a function of the ArF pulse number for the irradiation in DI (a) and air (b) and after RTA at 700°C for 2 minutes.

3.3 Photoluminescence measurement after ArF laser irradiation in air and DI water

Figure 9 shows the PL shift dependence on pulse number after ArF laser irradiating in air and DI water and RTA for 2 min at 700°C. The PL shift increases with pulse number and saturates at about 120 and 40 nm for the sites irradiated in

air and DI water, respectively. The greater PL shift in sample irradiated in air indicates that much greater amount of surface defects is created in that case.

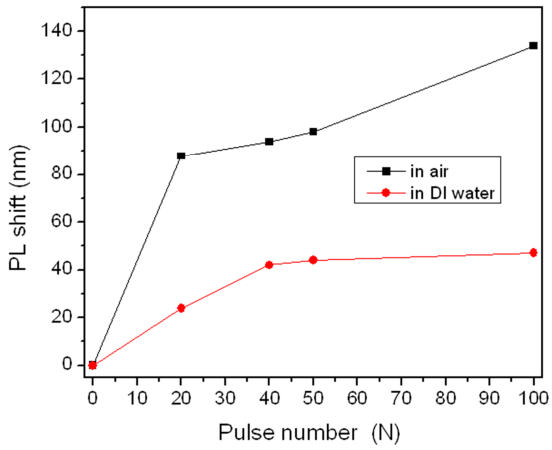

Figure 9. PL shift dependence on pulse number after ArF laser irradiation in air and DI water and RTA for 2 min at 700°C.

A comparison between Figure 6 and Figure 9 indicates that the PL shift dependence on the pulse number is proportional to the amount of InP oxides produced with the laser. It seems plausible that these oxides will react with P atoms outdiffusing from the QW microstructure during the RTA step. Consequently, the phosphorous vacancy diffusion towards the QW region is expected to contribute to the QWI effect.

4. CONCLUSION

In this paper, we have investigated chemical composition of the InP cap material deposited on top of InP/InGaAs/InGaAsP microstructures and irradiated with ArF laser at 82 mJ/cm^2 with up to 100 pulses. Following the RTA step, the irradiation that was carried out in air or DI water enabled us to observe bandgap blue shifting up to 120 nm. The PL shift in samples irradiated in air is generally greater than that in DI water. The XPS data have shown greater amount of InP oxides created during irradiation in air in comparison to the irradiation carried out in DI water. The results suggest that defects, such as group V vacancies created during P outdiffusion into the InP cap layer are primarily responsible for the amplitude of the QWI effect. We found that after RTA, the laser created InP oxides have diminished, indicating that our excimer laser QWI technique does not degrade electronic properties of the investigated QW microstructures.

5. ACKNOWLEDGEMENT

This work was supported by the Merit Scholarship program for Foreign Students from the Fonds de Recherche sur la Nature et les Technologies of Quebec, the Natural Science and Engineering Research Council of Canada the Plasma Québec and the Canada Research Chair in Quantum Semiconductors program (JJD). The help from the technical staff of the Centre de recherche en nanofabrication et en nanocaracterisation (CRN^2) is greatly appreciated.

REFERENCES

[1] Kim, H. S., Park, J. W., Oh, D. K., Oh, K. R., Kim, S. J. and Choi, I. H., "Quantum well intermixing of $In_{1-x}Ga_xAs/InP$ and $In_{1-x}Ga_xAs/In_{1-x}Ga_xAs_{1-y}P_y$ multiple-quantum-well structures by using the impurity-free vacancy diffusion technique," Semicond. Sci. Technol. 15, 1005 (2000).

[2] Jain, S., Sysak, M., Kurczveil, G. and Bowers, J. E., "Integrated hybrid silicon DFB laser-EAM array using quantum well intermixing," Optics Express 19 (14), 13692(2011).

[3] Ooi, B. S., Bryce, A. C., Marsh, J. H. and Roberts, J. S., "Effect of p and n doping on neutral impurity and dielectric cap induced quantum well intermixing in GaAs/AlGaAs structures," Semicond. Sci. Technol. 12 (1), 121 (1997).
[4] Laidig, W., Holonyak Jr, N., Camras, M., Hess, K., Coleman, J., Dapkus, P. and Bardeen, J., "Disorder of an AlAs GaAs superlattice by impurity diffusion," Appl. Phys. Lett. 38, 776 (1981).
[5] Teng, J., Dong, J., Chua, S., Lai, M., Foo, B., Thompson, D., Robinson, B., Lee, A., Hazell, J. and Sproule, I., "Controlled group V intermixing in InGaAsP quantum well structures and its application to the fabrication of two section tunable lasers," J. Appl. Phys. 92, 4330 (2002).
[6] Adachi, S., "Material parameters of $In_{1-x}Ga_xAs_yP_{1-y}$ and related binaries," J. Appl. Phys. 53 (12), 8775 (1982).
[7] Uchikoga, S. and Ibaraki, N., "Low temperature poly-Si TFT-LCD by excimer laser anneal," Thin Solid Films 383 (1), 19-24 (2001).
[8] Dubowski, J., "Laser-induced bandgap shifting for photonic device integration," US Patent #6,514,784 CA 2,331,567 (2003).
[9] Genest, J., Beal, R., Aimez, V. and Dubowski, J., "ArF laser-based quantum well intermixing in InGaAs/InGaAsP heterostructures," Appl. Phys. Lett. 93, 071106 (2008).
[10] Liu, N., Moumanis, K. and Dubowski, J. J., "Surface morphology of SiO_2 coated InP/InGaAs/InGaAsP microstructures following irradiation with the ArF and KrF excimer lasers," Proc. SPIE 7920, 79200C (2011).
[11] Pan, J., Wee, A., Huan, C., Tan, H. and Tan, K., "XPS studies on nitridation of InP (100) surface by ion beam bombardment," J. Phys. D: Appl. Phys. 29, 2997-3002 (1996).
[12] Xu, C. and Mei, T., "Inductively Coupled Argon Plasma-Enhanced Quantum-Well Intermixing: Cap Layer Effect and Plasma Process Influence," IEEE J. Quantum Elect., 45 (8), 920-926 (2009).
[13] Liu, N., Moumanis, K. and Dubowski, J. J., "Self-organized nano-cone arrays in InP/InGaAs/InGaAsP microstructures by irradiation with ArF and KrF excimer lasers," Proc. LPM2011, 11-033 (2011).
[14] Thomas III, J., Kaganowicz, G. and Robinson, J., "X ray Photoelectron Spectroscopy Analysis of Changes in InP and InGaAs Surfaces Exposed to Various Plasma Environments," J. Electrochem. Soci. 135, 1201 (1988).
[15] Pan, J., Tay, S., Huan, C. and Wee, A., "XPS study of incident angle effects on the ion beam modification of InP surfaces by 6 keV O 2," Surf. Inter. Anal. 27 (11), 993-997 (1999).
[16] Shibata, N. and Ikoma, H., "X-Ray photoelectron spectroscopic study of oxidation of InP," Jpn. J. Appl. Phys. 31, 3976-3980 (1992).
[17] Salvia, A. M. and Castle, J. E., "The intrinsic asymmetry of photoelectron peaks: dependence on chemical state and role in curve fitting," J. Electr. Spectrosc. 95 (1), 45-56 (1998).
[18] Nguyen, T. P., Lefrant, S., De Vos, S. and Gao, Y., "Interfacial reactions in poly (phenylene vinylene)-metal systems," Synth. Met. 84 (1-3), 659-660 (1997).
[19] Feurprier, Y., Cardinaud, C. and Turban, G., "Surface modification and etch product detection during reactive ion etching of InP in-plasma," Plasma Sources Sci. Technol. 6, 334 (1997).
[20] Jin, Z., Hashizume, T. and Hasegawa, H., "In Situ X-Ray Photoelectron Spectroscopy Study of Etch Chemistry of Methane-Based Reactive Ion Beam Etching of InP Using N2," Jpn. J. Appl. Phys. 40, 2757 (2001).
[21] Mikushkin, V., Sysoev, S. and Gordeev, Y., "Standardless XPS method for determining the chemical composition of multiphase compounds and its application to studies of InP plasma oxide nanofilms," Phys. Solid State 46 (10), 1830-1835 (2004).
[22] Hollinger, G., Bergignat, E., Joseph, J. and Robach, Y., "On the nature of oxides on InP surfaces," J. Vac. Sci. & Technol. A 3 (6), 2082-2088 (2009).
[23] Wilke, W. G., Hinkel, V., Theis, W. and Horn, K., "Surface core-level shifts on InP(110): Experiments and Madelung energy calculations," Phys. Rev. B 40 (14), 9824 (1989).
[24] Rosenberg, R. A., LaRoe, P. R., Rehn, V., Loubriel, G. M. and Thornton, G., "Soft-x-ray photoelectron-yield spectrum of InP(110) from 65 to 195 eV," Phys. Rev. B 28 (10), 6083 (1983).
[25] Han, I., Kim, E., Lee, J., Kim, S., Kang, K., Kim, Y., Lim, H. and Park, H., "Stability of sulfur-treated InP surface studied by photoluminescence and x-ray photoelectron spectroscopy," J. Appl. Phys. 81, 6986 (1997).
[26] Le Beuze, A., Lissillour, R., Quemerais, A., Agliz, D., Marchand, R. and Chermette, H., "Comprehensive study of the valence band of standard alkali-metal and indium phosphorus oxide salts through x-ray photoemission spectroscopy and extended Hukel theory tight-binding analysis: A contribution towards the elucidation of local order in oxides on InP surfaces," Phys. Rev. B 39 (15), 11055 (1989).
[27] Miller, D., Biesinger, M. and McIntyre, N., "Interactions of CO_2 and CO at fractional atmosphere pressures with iron and iron oxide surfaces: one possible mechanism for surface contamination," Surf. Interface Anal. 33 (4), 299-305 (2002).

[28] Gresch, R., Muller-Warmuth, W. and Dutz, H., "X-ray photoelectron spectroscopy of sodium phosphate glasses," J. Non-Crystal. Solids 34 (1), 127-136(1979).
[29] Ingrey, S., Lau, W., McIntyre, N. and Sodhi, R., "An x-ray photoelectron spectroscopy study on ozone treated InP surfaces," J. Vac. Sci. Technol. A 5, 1621 (1987).
[30] Stanowski, R., Voznyy, O. and Dubowski, J. J., "Finite element model calculations of temperature profiles in Nd: YAG laser annealed GaAs/AlGaAs quantum well microstructures," JLMN 1, 17-21 (2006).
[31] Chen, G., Visbeck, S., Law, D. and Hicks, R., "Structure-sensitive oxidation of the indium phosphide (001) surface," J. Appl. Phys. 91, 9362 (2002).
[32] Driad, R., McKinnon, W., Lu, Z. and McAlister, S., "Effect of UV-ozone oxidation on the device characteristics of InP-based heterostructure bipolar transistors," J. Electr. Mater. 29 (12), L33-L36 (2000).
[33] Schulze, P., Shaffer, S., Hance, R. and Utley, D., "Adsorption of water on rhenium studied by XPS," J. Vac. Sci. Technol. A 1 (1), 97-99 (1983).
[34] Yamaguchi, M. and Ando, K., "Thermal oxidation of InP and properties of oxide film," J. Appl. Phys. 51 (9), 5007-5012 (1980).
[35] Wolan, J. T. and Hoflund, G. B., "Chemical alteration of the native oxide layer on InP (111) by exposure to hyperthermal atomic hydrogen," J. Vac. Sci. Technol. A 16, 2546 (1998).
[36] Baranzahi, A., Spetz, A. L. and Lundstrom, I., "Reversible hydrogen annealing of metal oxide Silicon carbide devices at high temperatures," Appl. Phys. Lett. 67 3203 (1995).
[37] Gunawan, O., Ong, T. K., Chen, Y. W., Ooi, B. S., Lam, Y. L., Zhou, Y. and Chan, Y. C., "A theoretical analysis of quantum well intermixing using the pulsed laser irradiation technique in InGaAs/InGaAsP laser structure," Surf. Coat. Tech. 130 (1), 116-121 (2000).
[38] Abernathy, C., Pearton, S., Caruso, R., Ren, F. and Kovalchik, J., "Ultrahigh doping of GaAs by carbon during metalorganic molecular beam epitaxy," Appl. Phys. Lett.55 (17), 1750-1752 (1989).
[39] Akane, T., Sugioka, K., Midorikawa, K., Dubowski, J., Aoki, N. and Toyoda, K., "X-ray photoelectron spectroscopic study of KrF excimer laser nitrided InP surface," J. Appl. Phys. 90 (12), 5851-5855 (2001).